Int. J. Solids Structures Vol. 15, pp. 731–742

0020-7683/79/0901-0731/$02.00/0

NECKING OF A CYLINDRICAL BAR IN TENSION

MIRAN SAJE

University of Ljubljana, Faculty of Architecture, Civil Engineering and Survey, Jamova 2, 61000 Ljubljana, Yugoslavia

(*Received* 28 *August* 1978; *in revised form* 15 *March* 1979)

Abstract—The paper numerically analyses the necking of a cylindrical, elastic-plastic, strain-hardening bar in axisymmetric tension. Both geometric and material nonlinearities are taken into account. The Lagrangian formulation is used. The solution is obtained by a stepwise integration of the equilibrium equations, using the finite difference method. The results also include stress and strain distributions across the minimum bar section at various deformation stages up to 67% reduction of the bar's area. Comparisons with the results of previous investigators (Bridgman, Chen, Needleman, Norris) are also given.

1. INTRODUCTION

Since 1944, when Bridgman first determined the distribution of stresses in the narrowest section of the necked cylindrical bar in tension, there have been many other investigators of the problem, e.g. Davidenkov and Spiridonova[1], Parker *et al.*[2], Truszkowski and Jasieński[3], Thomason[4], Chen[5], Needleman[6], Norris *et al.*[7], all using different methods and all coming to more or less different results. The present analysis, again coming to new results, is hoped to contribute to the final solution of the problem.

The results are obtained by numerical integration of the equilibrium equations. The finite difference method is used. The nonlinear algebraic system of equations for nodal displacement increments, arising from a finite difference discretization, is solved iteratively. The comparison between the present and previous results is given for estimation and discussion.

2. BASIC EQUATIONS AND METHOD OF SOLUTION

Equilibrium equations

The equilibrium equations have the following nonlinear form when the Lagrangian description is used[8]

$$V_0: \quad [\bar{s}_0^{kl}(\delta_1{}^m + \bar{u}^m|_1)]|_k + \bar{f}^m = 0 \tag{1a}$$

$$S_0: \quad \bar{s}_0^{kl}(\delta_1{}^m + \bar{u}^m|_1)n_k{}^0 - \bar{p}_0{}^m = 0 \tag{1b}$$

$$(m, k, l = 1, 2, 3)$$

V_0 is the volume of the undeformed body bounded by the surface S_0; "$|_k$" means the covariant differentiation in the undeformed body with respect to the material coordinates $\theta_0{}^k$; $\bar{s}_0^{kl}$ symmetrical Kirchhoff stress tensor; $\bar{u}^m$ contravariant component of the displacement vector; $\delta_1{}^m$ Kronecker's symbol; $n_k{}^0$ covariant component of the unit normal to the undeformed surface S_0; $\bar{f}^m$ contravariant component of the volume force vector, and $\bar{p}_0{}^m$ is the contravariant component of the surface traction per unit of the undeformed area. The base vectors and covariant components of the metric tensor in the undeformed body are denoted by $\mathbf{g}_i$ and g_{ij} $(i, j = 1, 2, 3)$.

If a constitutive law is used the equations can be put into a form where the displacements are principal unknowns. For this purpose the decomposition of the components of stresses, displacements and forces is made:

$$\bar{s}_0^{kl} = s_0^{kl} + \Delta s_0^{kl} \tag{2a}$$

$$\bar{u}^k = u^k + \Delta u^k \tag{2b}$$

$$\bar{p}_0{}^k = p_0{}^k + \Delta p_0{}^k \tag{2c}$$

$$\bar{f}^k = f^k + \Delta f^k \tag{2d}$$

where s_0^{kl} and u^k are known and correspond to forces $p_0{}^k$ and f^k, while Δs_0^{kl} and Δu^k are unknown increments, corresponding to $\Delta p_0{}^k$ and Δf^k. Δs_0^{kl} is then expressed with the displacement increments using the constitutive law for elastic–plastic materials

$$\Delta s_0^{kl} = C_0^{klpr} \Delta \gamma_{pr} \tag{3}$$

where

$$\Delta \gamma_{pr} = \frac{1}{2}[(\delta_p{}^n + u^n|_p)\Delta u_n|_r + (\delta_r{}^n + u^n|_r)\Delta u_n|_p] + \frac{1}{2}\Delta u_n|_r \Delta u^n|_p \tag{4}$$

is the Lagrangian strain tensor increment and C_0^{klpr} the constitutive tensor depending on strains and stresses. The constitutive equations will be discussed later. Using (2)–(4) in (1), the following set of equations is obtained:

$$V_0: \quad (K^{krmn}\Delta u_n|_r)|_k + [\tfrac{1}{2} C_0^{klpr}(\delta_1{}^m + u^m|_1)\Delta u^n|_p \Delta u_n|_r]|_k + [s_0^{kl}(\delta_1{}^m + u^m|_1)]|_k + \bar{f}^m = 0 \tag{5a}$$

$$S_0: \quad K^{krmn}\Delta u_n|_r n_k{}^0 + \frac{1}{2} C_0^{klpr}(\delta_1{}^m + u^m|_1)\Delta u^n|_p \Delta u_n|_r n_k{}^0 + s_0^{kl}(\delta_1{}^m + u^m|_1) n_k{}^0 - \bar{p}_0{}^m = 0 \tag{5b}$$

$$K^{krmn} = s_0^{kr} g^{mn} + C_0^{klpr}(\delta_1{}^m + u^m|_1)(\delta_p{}^n + u^n|_p). \tag{6}$$

These are nonlinear differential equations for unknown displacement increments Δu_i; when solved, the displacements can easily be obtained:

$$\bar{u}_m = u_m + \Delta u_m. \tag{7}$$

This makes it possible to compute the Lagrangian strain tensor components, using the formula

$$\bar{\gamma}_{pr} = \frac{1}{2}(\bar{u}_p|_r + \bar{u}_r|_p + \bar{u}_n|_p \bar{u}^n|_r) \tag{8}$$

the covariant and contravariant components of the deformed metric tensor, using the relations

$$\bar{G}_{pr} = 2\bar{\gamma}_{pr} + g_{pr} \tag{9a}$$

$$\bar{G}_{pn}\bar{G}^{nr} = \delta_p{}^r \tag{9b}$$

and the Kirchhoff stresses $\bar{s}_0^{kl}$, using eqns (2a) and (3).

The physical (Cauchy) components of the true stresses are determined by the relation

$$\sigma_{ij} = \sqrt{\left(\frac{g}{\bar{G}}\right)} \sqrt{\left(\frac{g_{ii}}{g^{ii}}\right)} \sum_{p,r} (\delta_p{}^i + \bar{u}^i|_p)(\delta_r{}^j + \bar{u}^j|_r)\bar{s}_0^{pr} \tag{10}$$

where g and $\bar{G}$ are the determinants of the undeformed and deformed metric tensors g_{ij} and $\bar{G}_{ij}$.

Following the finite difference method, the integration region is divided into a rectangular net and the differential equations (5a,b) are written in finite difference form at corresponding nodes. The resulting system of nonlinear algebraic equations for unknown nodal displacement increments ΔU_{mM} (the index M indicates the M-th node and goes from 1 to the total number of nodes) is solved iteratively by subsequently solving the linearized systems of equations (5)

$$V_0: \quad D\{(K^{krmn}\Delta u_n|_r)|_k\}^{(\alpha)} = -D\{[s_0^{kl}(\delta_1{}^m + u^m|_1)]|_k + \bar{f}^m\}^{(\alpha)} \tag{11a}$$

$$S_0\colon D\{(K^{krmn}\Delta u_n|_r n_k^0)\}^{(\alpha)} = -D\{s_0^{kl}(\delta_1{}^m + u^m|_1)n_k^0 - \bar{p}_0{}^m\}^{(\alpha)} \tag{11b}$$

$$(\alpha = 0, 1, 2, 3, \ldots)$$

$$\Delta U_{mM} = \sum_{\alpha} \Delta U_{mM}^{(\alpha)} \tag{11c}$$

where "D" and (α) designate that the expression is written in the finite difference form and computed at the known values of the α-th iteration. The terms on the right-hand sides of eqns (11a),(b) are equal to those on the left-hand sides of eqns (1a),(b). For this reason, the solution approaches the equilibrium state, if they approach zero. This is tested by computing norm of the r.h.s. of (11a),(b) after each iteration, and when it is smaller than an arbitrary small value, the iteration is interrupted. Nodal displacements, strains and stresses at the loads $\bar{p}_0{}^m$ and $\bar{f}^m$ are then computed. We also tested the norms of the $\Delta U_{mM}^{(\alpha)}$ vectors and found that they were usually less decisive.

We use the usual (h^2) difference operators. Symmetric operators are used in the interior points and nonsymmetric at the boundary. The actual finite difference scheme of eqn (11a) for $m = 1$ and $m = 3$, applied at axisymmetric stress and strain state and with cylindrical coordinates used, is given in the Appendix.

Constitutive equations

The present analysis employs the constitutive equations, which were derived in [9]; only an abstract of that paper is given here. The theory of general elastic–plastic materials at finite strains, similar to that of Green and Naghdi (1965), is derived first. Next, the relation between the stress rate $\dot{s}_0^{ij}$ and the strain rate d_{ij}, which depends on four experimentally determined tensor functions, is deduced. For the purpose of the present analysis these functions are chosen in such a way that within the supposition of material incompressibility the constitutive equations reduce to the known equations of the generalized Prandtl–Reuss (or $\mathcal{J}_2$) flow theory with Mises yield condition (see [5]).

The theory uses the term "effective stress" defined by

$$f = \sqrt{\left(\frac{3}{2} G_{jk} G_{il} t^{ij} t^{kl}\right)} \tag{12}$$

where the contravariant components of the stress deviator tensor t^{ij} are given by the relation

$$t^{ij} = \tau^{ij} - \frac{1}{3} G^{ij} G_{mn} \tau^{mn} \tag{13}$$

in which

$$\tau^{ij} = \sqrt{\left(\frac{g}{G}\right)} s_0^{ij} \tag{14}$$

is Euler's stress tensor. The Mises yield condition demands that "f" is equal to the function κ, defined as either the maximum value of "f" over the stress history, or the initial yield stress, whichever is greater. Then [9]:

$$\Delta s_0^{ij} = C_0^{ijpr} \Delta \gamma_{pr} \tag{15a}$$

$$C_0^{ijpr} = \lambda G^{ij} G^{pr} + \mu(G^{ir} G^{jp} + G^{ip} G^{jr}) - s_0^{jp} G^{ir} - s_0^{ip} G^{jr} + \psi \left(\frac{3\mu}{f}\right)^2 t^{ij} t^{pr} \tag{15b}$$

$$\lambda = \frac{\nu E}{(1+\nu)(1-2\nu)} \tag{15c}$$

$$\mu = \frac{E}{2(1+\nu)} \tag{15d}$$

$$\frac{1}{\psi} = -\left(3\mu + \frac{1}{\frac{1}{E_p} - \frac{1}{E}}\right) \qquad \text{if } f = \kappa \text{ and } \dot{f} > 0 \qquad (15e)$$

(loading in the plastic region)

$$\psi = 0 \qquad \text{if } f = \kappa \text{ and } \dot{f} \leqq 0 \qquad (15f)$$

(unloading in the plastic region)
or $f < \kappa$
(elastic region).

The quantities E (elastic modulus) and E_p (plastic modulus) are determined from a tangent of a true stress vs logarithmic axial strain curve in uniaxial tension, while ν is Poisson's ratio. The Ramberg–Osgood representation for uniaxial tensile true stress-logarithmic strain curve is used here. For this representation

$$\frac{1}{E_p} = \frac{1}{E} + \frac{3}{7} n \left(\frac{f}{\sigma_s}\right)^{n-1} \qquad (16)$$

where σ_s and n are material constants.

The elastic–plastic law (15a) has two branches, elastic and plastic, and this complicates the numerical procedure. For a given load increment some nodes remain elastic or plastic, while others pass from elastic to plastic region or vice versa. This is tested in each iteration. If unloading is detected in at least one node, the matrix of the system (11a),(b) should be reformed, using elastic stress–strain matrices at such node(s) and the iteration should be repeated. For convenience we simplified the procedure and repeated only the first iteration, while in the subsequent iterations the elastic law was taken for the unloaded nodes. When the solution is obtained, the stress state is tested and used for the determination of starting constitutive matrices for the computation of the matrix of the system (11) in the next load increment. When certain nodes become plastic, the iteration is not repeated; the calculations of stresses however take into account that some stresses develop in elastic region and some in plastic.

3. RESULTS AND DISCUSSION

Formulation of the necking problem

The local contraction in a real bar appears because of imperfect material and geometrical structure. This structure is usually not known, so it is impossible to predict the location of the contraction. In numerical analyses the problem is therefore simplified and certain simple distributions of imperfections are chosen. Previous numerical analyses took a materially homogenous but geometrically imperfect bar with free ends [5–7] or materially and geometrically perfect bar with clamped ends [6]. In the present analysis the latter possibility was used because of computational advantages. In this case the contraction of the bar is inhomogenous from the very beginning of loading, while the neck is located in the middle of the bar.

The bar is assumed to be axisymmetric with respect to z-axis and symmetric with respect to the middle plane $z = 0$. This suggests the use of cylindrical coordinates r, φ, z. Only one fourth of the specimen needs to be dealt with.

Geometric, material and loading characteristics and the finite difference net employed are shown in Fig. 1. The initial half-length to initial bar radius ratio is $L/R = 2$. The strain-hardening exponent in Ramberg–Osgood law is $n = 8$, the ratio σ_s/E is 0.0072 and Poisson's ratio is $\nu = 1/3$. The finite difference net has 91 nodes.

The bar was subjected to the prescribed uniform axial displacement U at the bar ends. U rose in small increments (as given in Fig. 1) and at each stage of the displacement the complete analysis was carried out. The elongation was interrupted at $U = 0.37525\ L$, when the procedure began to diverge. The results are presented as far as $U/L = 0.35$ (or equivalently $S/S_0 = 0.33$) where, to our feeling, the accuracy is still satisfactory.

(a) Geometry: L/R = 2.

(b) Material: Ramberg-Osgood law; E = 210 000 ; ν = 1/3 ;
n = 8 ; σ_s = 0,0072 E.

(c) Loading: Boundary displacement increments:

$\frac{U}{L}$ = 0,000 - 0,212 (ΔU = 0,002 L)
0,212 - 0,268 (ΔU = 0,001 L)
0,268 - 0,37525 (ΔU = 0,00075 L)

(d) Number of nodes: 91.

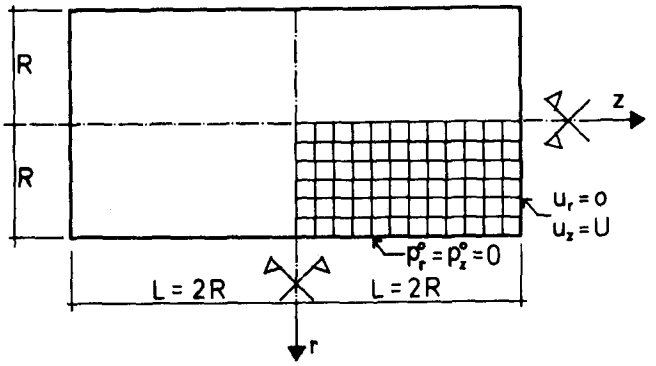

Fig. 1. Geometric, material and loading characteristics of cylindrical bar. Finite difference net.

Results and discussion

Figure 2(a) shows axial force (P) vs area reduction (S/S_0) curves for a perfect, elastic–plastic bar (curve 1), where the local contraction never appears, and for the here analysed bar (curve 2). Axial force vs engineering axial strain (U/L) curves are shown in Fig. 2(b). Note the different position of the perfect bar curves with respect to the curves of a necked bar in both figures.

When the axial force decreases, the effective stress near the ends begins to decrease and plastic unloading starts. This implies that in the unloaded zone the area contraction stops, while the cross section at the neck contracts even faster. For this reason the axial force decreases further, causing larger unloaded zones at the ends and localizing the plastic deformations more to the neck. This is shown in Fig. 3 where spreading of plastic loading and unloading zones is plotted in the undeformed bar. The nodes in the plastic unloading zone in this figure can be considered as elastic, yet with a new, higher yield stress.

The global shapes of the necked bar at three different deformation stages are shown in Fig. 4(a)–(c). The deformed (or "spatial") pictures of the originally square net give a good insight into the local deformations.

The distributions of physical components of Lagrangian strains at various deformation stages are given in Fig. 5(a), while physical components of stresses are given in Fig. 5(b). Strains and stresses decrease smoothly from the axis of symmetry to the surface. Observe the agreement between the stress distributions of the present analysis and those resulting from the Bridgman's formulae, in which the curvature radii from this analysis are put. The distributions of the circumferential stress component show increasing compression on the surface until $S/S_0 = 0.66$, after which this surface component decreases and becomes tensile at $S/S_0 = 0.43$. The phenomenon of increasing and decreasing of surface $\sigma_{\varphi\varphi}$ stress agrees with experiments of Parker *et al.*[2] and with computations of Norris *et al.*[7]. The transition to tension has been displayed also by Parker *et al.*

Figure 6 shows the curve of the normal longitudinal physical stress component in the central point of the bar vs area reduction (S/S_0). Note that the curve starts to decrease at $S/S_0 = 0.46$.

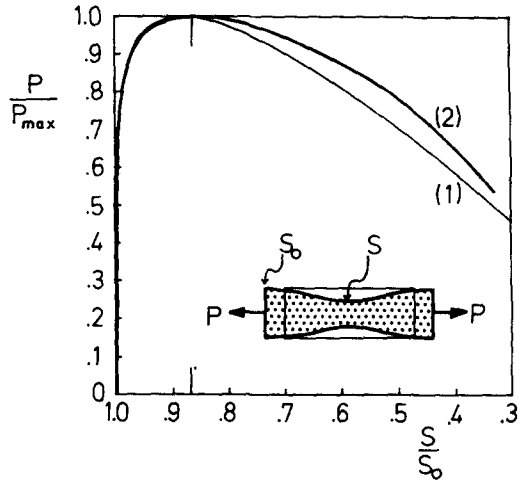

(a)

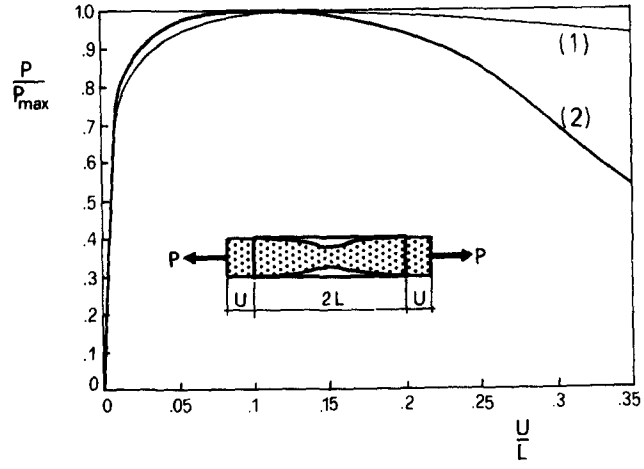

(b)

Fig. 2. (a) Axial force (P) vs area reduction (S/S_0); (b) Axial force (P) vs engineering axial strain (U/L). (1) Ideal bar, (2) present bar.

4. COMPARISONS WITH PREVIOUS SOLUTIONS

Bridgman as well as Davidenkov and Spiridonova pay attention to the minimum section only. They both assume that the stress components σ_{rr} and $\sigma_{\varphi\varphi}$ are equal; they derive the r-th component of the equilibrium equation in terms of principal stresses ($\sigma_r = \sigma_\varphi, \sigma_z$). They both reach the same result

$$V: \quad \frac{d\sigma_r}{dr} + \frac{1}{\rho}(\sigma_z - \sigma_r) = 0 \tag{17}$$

whereas for $\rho(r)$, the curvature radius of the trajectory of the principal stress σ_z at "r", they propose different formulae. Bridgman suggests the expression

$$\rho = \frac{R + \frac{a}{2}\left[1 - \left(\frac{r}{a}\right)^2\right]}{\frac{r}{a}} \tag{18}$$

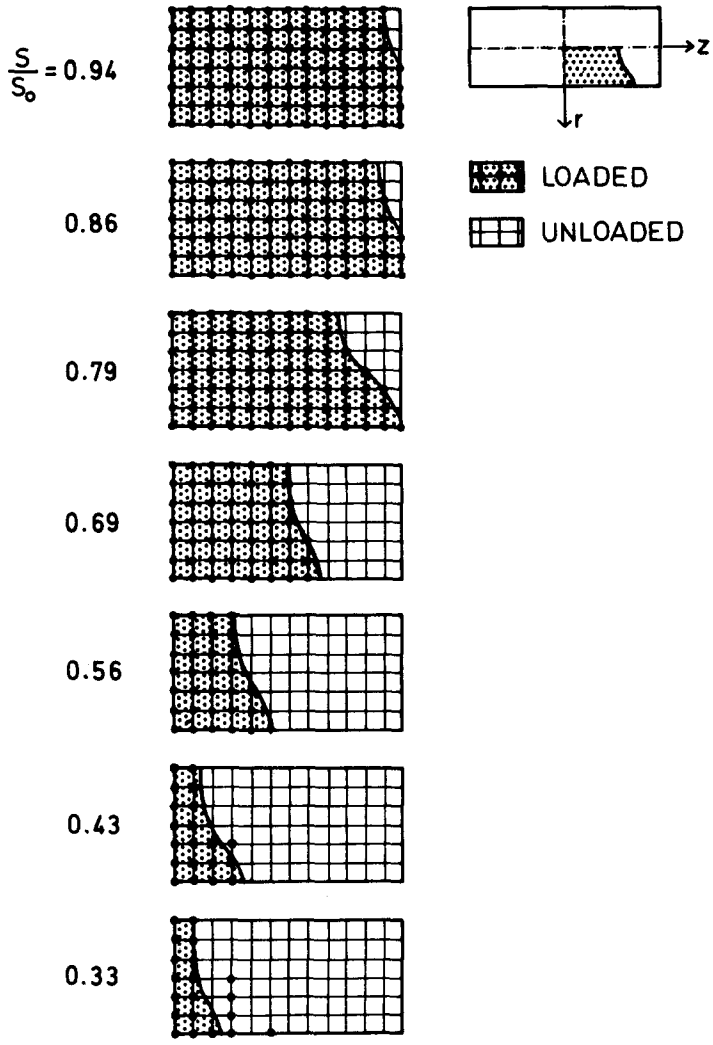

Fig. 3. Spreading of plastic loading and plastic unloading zones.

which results from the assumption that the trajectories are circles. Here a means radius of minimum bar section and R radius of curvature of contour at minimum section. Davidenkov and Spiridonova, with some experimental evidence, take

$$\rho = \frac{aR}{r}. \tag{19}$$

With (18) or (19) and Mises yield condition

$$\sigma_z - \sigma_r = \text{constant},$$

the integration of (17) is simple, giving the known results. For $\sigma_{rr} = \sigma_{\varphi\varphi}$ and a non-hardening material they would be correct if ρ were correct. The comparison of (18), (19) and ρ, obtained by the present analysis at $S/S_0 = 0.43$, shows agreement with Bridgman's proposal, but not with that of Davidenkov and Spiridonova. The stress distributions of the present method are therefore compared only with Bridgman's results, in which we put numerically obtained curvature and neck radii.

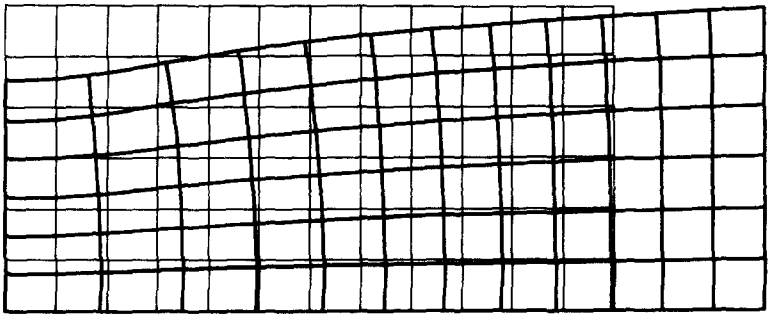

(a)

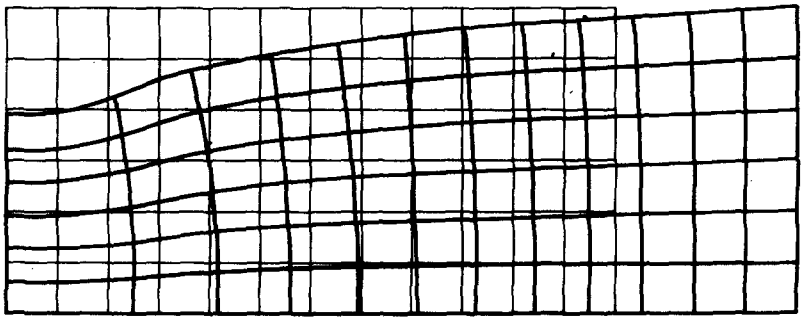

(b)

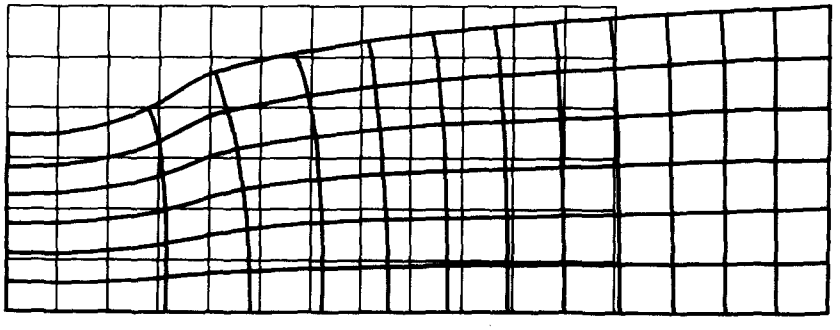

(c)

Fig. 4. Shapes of the necked bar at three stages of deformation: (a) $S/S_0 = 0.56$; (b) $S/S_0 = 0.43$; (c) $S/S_0 = 0.33$.

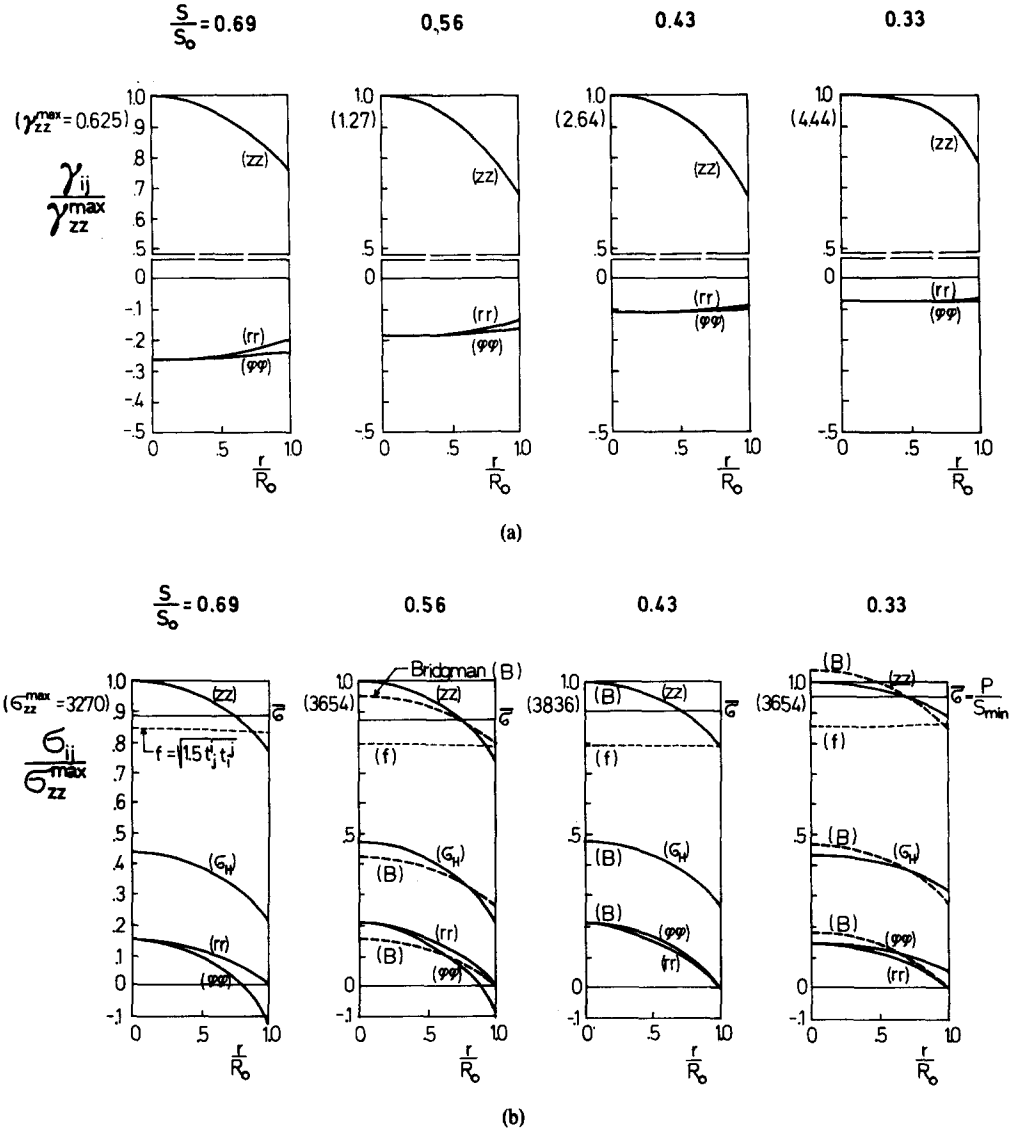

Fig. 5. (a) Distribution of physical components of Lagrangian strains at the neck ($z = 0$); (b) Distribution of physical components of stresses at the neck ($z = 0$). σ_H – hydrostatic stress.

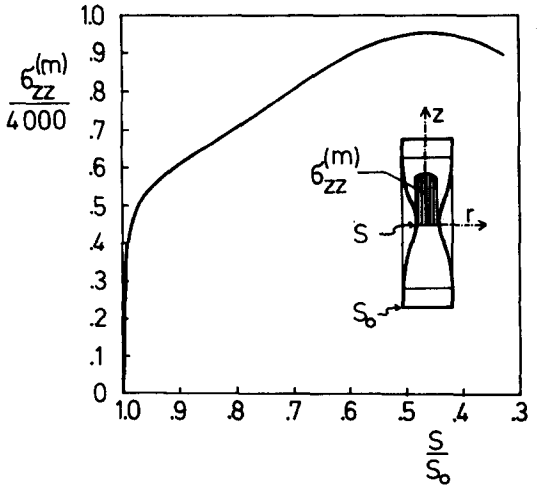

Fig. 6. Longitudinal stress component $\sigma_{zz}^{(m)}$ in the central point of the bar vs area reduction (S/S_0).

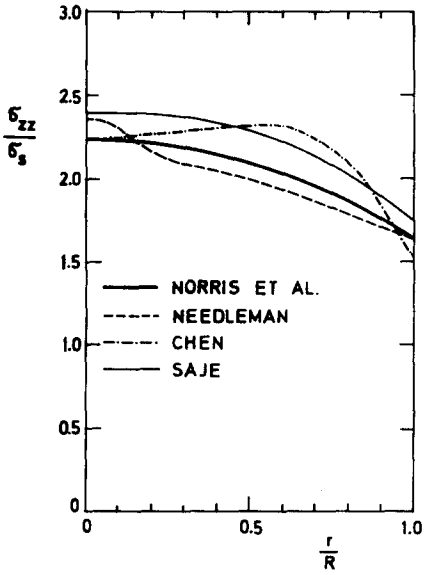

Fig. 7. Distributions of stresses by Chen[5], Needleman[6] and Norris *et al.*[7] compared with the distributions by the present analysis at $S/S_0 \doteq 0.59$.

The numerical results show that σ_{rr} and $\sigma_{\varphi\varphi}$ are equal only once during the whole deformation (at $S/S_0 = 0.43$, Fig. 5b), and that at this stage the stress distributions by both methods coincide. As expected there is not such a good agreement at other stages.

Chen[5], Needleman[6] and Norris *et al.*[7] made calculations similar to those presented here. They all formulated the problem in a different way and applied different numerical procedures. Figure 7 shows the comparison of some of the published results for σ_{zz} stress at $S/S_0 \doteq 0.59$. The oscillating distribution given by Chen is not confirmed by the present solution. The discrepancy has however been expected since his solution does not satisfy the boundary condition $\sigma_{rr} = 0$ at $r = R$, $z = 0$, but not to such extent. It is however interesting that similar oscillations of stresses are found by the present method if a coarser finite difference net is used (3×6 instead of 6×12). That points to the numerical sensitivity of the problem. The effect of shifting the maximum stress off the axis of the bar in Chen's solution is incompatible with the effect of the development of the sharp stress peak on the axis, obtained by Needleman. Disregarding this peak, Needleman's shape of stress distribution agrees in general with ours. The shape given by Norris *et al.* is similar to the present one, except that the present curve lies completely above their curve, which is due to different material characteristics, as discussed by Norris *et al.*

The strain distributions are similar in shape in all cases and need not be compared here.

5. ADDITIONAL REMARKS

The following statements have not been noted in previous investigations:

(1) The distributions of the radial and the circumferential stress components in the narrowest section are equal only at one stage during the process of necking. This stage will be called "the critical stage".

(2) At this stage Bridgman's formulae give accurate results.

(3) The longitudinal normal stress component in the central point of the bar increases at first until it reaches the maximum value at a certain deformation stage which occurs a little bit earlier than the critical stage. After that it decreases.

(4) When the critical stage is reached, the radius of the curvature of the neck profile starts to increase, while stress and strain concentration factors begin to decrease. This means that the necked portion tends to elongate and to behave like a perfect bar. In a metal bar this would not really happen since fracture would take place earlier. The present study does not

consider fracture and therefore can not predict when a bar breaks. Nevertheless the results have practical value since they are essential for any fracture study.

Acknowledgement—To Prof. D. Jurišić of Faculty for Architecture, Civil Engineering and Survey, University of Ljubljana, for many helpful discussions during the course of this study.

REFERENCES

1. N. N. Davidenkov and N. I. Spiridonova, Mechanical methods of testing analysis of the state of stress in the neck of a tension test specimen. *Proc. Am. Soc. Test. Mat.* **46**, 1147 (1946).
2. E. R. Parker, H. E. Davis and A. E. Flanigan, A study of the tension test. *Proc. Am. Soc. Test. Mat.* **46**, 1159 (1946).
3. W. Truszkowski and Z. Jasieński, An experimental analysis of the strain distribution in the neck of a tensile specimen. *J. Inst. Metals* **92**, 225 (1963).
4. P. F. Thomason, An analysis of necking in axisymmetric tension specimens. *Int. J. Mech. Sci.* **11**, 481 (1969).
5. W. H. Chen, Necking of a bar. *Int. J. Solids Structures* **7**, 685 (1971).
6. A. Needleman, A numerical study of necking in circular cylindrical bars. *J. Mech. Phys. Solids* **20**, 111 (1972).
7. D. M. Norris, Jr., B. Moran, J. K. Scudder and D. F. Quiñones, A computer simulation of the tension test. *J. Mech. Phys. Solids* **26**, 1 (1978).
8. C. Eringen, *Nonlinear Theory of Continuous Media.* McGraw-Hill (1962).
9. M. Sage, Elastic–plastic constitutive equations at large strains (in Serbo-Croatian). *XIV-th Yugoslav Symp. Rat. Appl. Mech.* A2–13, 221 (1978).
10. A. E. Green and P. M. Naghdi, A general theory of an elastic–plastic continuum. *Arch. Rat. Mech. Anal.* **18**, 251 (1965).
11. P. W. Bridgman, *Studies in Large Plastic Flow and Fracture.* McGraw-Hill (1952).

APPENDIX

Finite difference schemes of eqn (11*a*)

Notation

"$_{,r}$" partial derivative with respect to r;
"$_{,z}$" partial derivative with respect to z;
u_r, u_z r and z components of displacement vector;
h net characteristic;
C^{ij} components of constitutive matrix:

$$\begin{Bmatrix} \Delta s_0^{rr} \\ \Delta s_0^{\varphi\varphi} \\ \Delta s_0^{zz} \\ \Delta s_0^{rz} \end{Bmatrix} = \begin{bmatrix} C^{11} & C^{12} & C^{13} & C^{14} \\ C^{21} & C^{22} & C^{23} & C^{24} \\ C^{31} & C^{32} & C^{33} & C^{34} \\ C^{41} & C^{42} & C^{43} & C^{44} \end{bmatrix} \begin{Bmatrix} \Delta\gamma_{rr} \\ \Delta\gamma_{\varphi\varphi} \\ \Delta\gamma_{zz} \\ 2\Delta\gamma_{rz} \end{Bmatrix}$$

$K_{ij}, L_{ij}, M_{ij}, N_{ij}$ auxiliary symbols:

$$K_{11} = C^{11}(1+u_{r,r})^2 + C^{41}(1+u_{r,r})u_{r,z} + C^{14}(1+u_{r,r})u_{r,z} + C^{44}(u_{r,z})^2 + s_0^{rr}$$
$$K_{13} = C^{14}(1+u_{r,r})^2 + C^{44}(1+u_{r,r})u_{r,z} + C^{13}(1+u_{r,r})u_{r,z} + C^{43}(u_{r,z})^2 + s_0^{rz}$$
$$K_{31} = C^{11}(1+u_{r,r})u_{z,r} + C^{41}u_{r,z}u_{z,r} + C^{14}(1+u_{r,r})(1+u_{z,z}) + C^{44}(1+u_{z,z})u_{r,z}$$
$$K_{33} = C^{14}(1+u_{r,r})u_{z,r} + C^{44}u_{r,z}u_{z,r} + C^{13}(1+u_{r,r})(1+u_{z,z}) + C^{43}(1+u_{z,z})u_{r,z}$$
$$K_1 = [C^{12}(1+u_{r,r}) + C^{42}u_{r,z}](r+u_r)$$
$$L_{11} = K_{13}$$
$$L_{13} = C^{44}(1+u_{r,r})^2 + C^{34}(1+u_{r,r})u_{r,z} + C^{43}(1+u_{r,r})u_{r,z} + C^{33}(u_{r,z})^2 + s_0^{zz}$$
$$L_{31} = C^{41}(1+u_{r,r})u_{z,r} + C^{31}u_{r,z}u_{z,r} + C^{44}(1+u_{r,r})(1+u_{z,z}) + C^{34}(1+u_{z,z})u_{r,z}$$
$$L_{33} = C^{44}(1+u_{r,r})u_{z,r} + C^{34}u_{r,z}u_{z,r} + C^{43}(1+u_{r,r})(1+u_{z,z}) + C^{33}(1+u_{z,z})u_{r,z}$$
$$L_1 = [C^{42}(1+u_{r,r}) + C^{32}u_{r,z}](r+u_r)$$
$$M_{11} = K_{31}$$
$$M_{13} = L_{31}$$
$$M_{31} = C^{11}(u_{z,r})^2 + C^{41}(1+u_{z,z})u_{z,r} + C^{14}(1+u_{z,z})u_{z,r} + C^{44}(1+u_{z,z})^2 + s_0^{rr}$$
$$M_{33} = C^{14}(u_{z,r})^2 + C^{44}(1+u_{z,z})u_{z,r} + C^{13}(1+u_{z,z})u_{z,r} + C^{43}(1+u_{z,z})^2 + s_0^{rz}$$
$$M_1 = [C^{12}u_{z,r} + C^{42}(1+u_{z,z})](r+u_r)$$
$$N_{11} = K_{33}$$
$$N_{13} = L_{33}$$
$$N_{31} = M_{33}$$
$$N_{33} = C^{44}(u_{z,r})^2 + C^{34}(1+u_{z,z})u_{z,r} + C^{43}(1+u_{z,z})u_{z,r} + C^{33}(1+u_{z,z})^2 + s_0^{zz}$$
$$N_1 = [C^{42}u_{z,r} + C^{32}(1+u_{z,z})](r+u_r).$$

r-th component:

$(\Delta U_{rM}^{(\alpha)})$

$-(K_{13}+L_{11})$	$4L_{13} + 2h(K_{13,r}+L_{13,z}+\frac{1}{r}K_{13})$	$K_{13}+L_{11}$
$4K_{11} - 2h(K_{11,r}+L_{11,z}+\frac{1}{r}K_{11})$	$-8(K_{11}+L_{13})+4h^2[K_{1,r}+L_{1,z}+\frac{1}{r}K_1-C^{22}(r+u_r)^2-s_o^{\varphi\varphi}$	$4K_{11} + 2h(K_{11,r}+L_{11,z}+\frac{1}{r}K_{11})$
$K_{13}+L_{11}$	$4L_{13} - 2h(K_{13,r}+L_{13,z}+\frac{1}{r}K_{13})$	$-(K_{13}+L_{11})$

+

$(\Delta U_{zM}^{(\alpha)})$

$-(K_{33}+L_{31})$	$4L_{33}+2h(K_{33,r}+ L_{33,z}-N_1+\frac{1}{r}K_{33})$	$K_{33}+L_{31}$
$4K_{31}-2h(K_{31,r}+ L_{31,z}-M_1+\frac{1}{r}K_{31})$	$-8(K_{31}+L_{33})$	$4K_{31}+2h(K_{31,r}+ L_{31,z}-M_1+\frac{1}{r}K_{31})$
$K_{33}+L_{31}$	$4L_{33}-2h(K_{33,r}+ L_{33,z}-N_1+\frac{1}{r}K_{33})$	$-(K_{33}+L_{31})$

=

$$-4h^2\{[s_o^{rr}(1+u_{r,r})+s_o^{rz}u_{r,z}]_{,r}+[s_o^{zr}(1+u_{r,r})+s_o^{zz}u_{r,z}]_{,z}+\frac{1}{r}[s_o^{rr}(1+u_{r,r})+s_o^{rz}u_{r,z}]-(r+u_r)s_o^{\varphi\varphi}\}$$

z-th component:

$(\Delta U_{rM}^{(\alpha)})$

$-(M_{13}+N_{11})$	$4N_{13}+2h(M_{13,r}+ N_{13,z}+\frac{1}{r}M_{13}+N_1)$	$M_{13}+N_{11}$
$4M_{11}-2h(M_{11,r}+ N_{11,z}+\frac{1}{r}M_{11}+M_1)$	$-8(M_{11}+N_{13})+4h^2(M_{1,r}+N_{1,z}+\frac{1}{r}M_1)$	$4M_{11}+2h(M_{11,r}+ N_{11,z}+\frac{1}{r}M_{11}+M_1)$
$M_{13}+N_{11}$	$4N_{13}-2h(M_{13,r}+ N_{13,z}+\frac{1}{r}M_{13}+N_1)$	$-(M_{13}+N_{11})$

+

$(\Delta U_{zM}^{(\alpha)})$

$-(M_{33}+N_{31})$	$4N_{33} + 2h(M_{33,r}+N_{33,z}+\frac{1}{r}M_{33})$	$M_{33}+N_{31}$
$4M_{31} - 2h(M_{31,r}+N_{31,z}+\frac{1}{r}M_{31})$	$-8(M_{31}+N_{33})$	$4M_{31} + 2h(M_{31,r}+N_{31,z}+\frac{1}{r}M_{31})$
$M_{33}+N_{31}$	$4N_{33} - 2h(M_{33,r}+N_{33,z}+\frac{1}{r}M_{33})$	$-(M_{33}+N_{31})$

=

$$-4h^2\{[s_o^{rr}u_{z,r}+s_o^{rz}(1+u_{z,z})]_{,r}+[s_o^{zr}u_{z,r}+s_o^{zz}(1+u_{z,z})]_{,z}+\frac{1}{r}[s_o^{rr}u_{z,r}+s_o^{rz}(1+u_{z,z})]\}$$